Extending the Treatment of Backbone Energetics in Protein Force Fields: Limitations of Gas-Phase Quantum Mechanics in Reproducing Protein Conformational Distributions in Molecular Dynamics Simulations

ALEXANDER D. MACKERELL, JR.,[1] MICHAEL FEIG,[2] CHARLES L. BROOKS III[2]
[1]*Department of Pharmaceutical Sciences, School of Pharmacy, University of Maryland, 20 Penn Street, Baltimore, Maryland 21201*
[2]*Department of Molecular Biology (TPC6), The Scripps Research Institute, 10550 Torrey Pines Road, La Jolla, California 92037*

Received 19 March 2004; Accepted 29 March 2004
DOI 10.1002/jcc.20065
Published online in Wiley InterScience (www.interscience.wiley.com).

Abstract: Computational studies of proteins based on empirical force fields represent a powerful tool to obtain structure–function relationships at an atomic level, and are central in current efforts to solve the protein folding problem. The results from studies applying these tools are, however, dependent on the quality of the force fields used. In particular, accurate treatment of the peptide backbone is crucial to achieve representative conformational distributions in simulation studies. To improve the treatment of the peptide backbone, quantum mechanical (QM) and molecular mechanical (MM) calculations were undertaken on the alanine, glycine, and proline dipeptides, and the results from these calculations were combined with molecular dynamics (MD) simulations of proteins in crystal and aqueous environments. QM potential energy maps of the alanine and glycine dipeptides at the LMP2/cc-pVxZ//MP2/6-31G* levels, where x = D, T, and Q, were determined, and are compared to available QM studies on these molecules. The LMP2/cc-pVQZ//MP2/6-31G* energy surfaces for all three dipeptides were then used to improve the MM treatment of the dipeptides. These improvements included additional parameter optimization via Monte Carlo simulated annealing and extension of the potential energy function to contain peptide backbone ϕ, ψ dihedral crossterms or a ϕ, ψ grid-based energy correction term. Simultaneously, MD simulations of up to seven proteins in their crystalline environments were used to validate the force field enhancements. Comparison with QM and crystallographic data showed that an additional optimization of the ϕ, ψ dihedral parameters along with the grid-based energy correction were required to yield significant improvements over the CHARMM22 force field. However, systematic deviations in the treatment of ϕ and ψ in the helical and sheet regions were evident. Accordingly, empirical adjustments were made to the grid-based energy correction for alanine and glycine to account for these systematic differences. These adjustments lead to greater deviations from QM data for the two dipeptides but also yielded improved agreement with experimental crystallographic data. These improvements enhance the quality of the CHARMM force field in treating proteins. This extension of the potential energy function is anticipated to facilitate improved treatment of biological macromolecules via MM approaches in general.

© 2004 Wiley Periodicals, Inc. J Comput Chem 25: 1400–1415, 2004

Key words: *ab initio*; CMAP; molecular dynamics; dihedral angles; empirical force field; molecular mechanics

Introduction

Theoretical studies of proteins and other biological macromolecules are dominated by empirical force field based approaches.[1,2] Consistent with this is the availability of a number of empirical force fields for proteins including CHARMM19[3] and 22,[4] OPLS,[5] AMBER,[6] GROMOS,[7] ECEPP,[8] and TINKER,[9] among others. Although these force fields have been successfully applied to a wide variety of proteins, inherent limitations to their accuracy remain. For example, MD simulations of polypeptides have indicated the existence of π helices in peptides in solution and in lipid environments,[10–15] a phenomena we have recently shown to be

Correspondence to: A.D. MacKerell, Jr.; e-mail: amackere@rx.umaryland.edu

Contract/grant sponsor: the NIH; contract/grant numbers: GM51501 (to A.D.M.) GM37554 and RR12255 (to C.L.B.)

Contact/grant sponsor: DOD; contract/grant number: DAMD17-03-2-0012 (to C.LB.)

This article includes Supplementary Material available from the authors upon request or via the Internet at http://www.interscience.wiley.com/jpages/0192-8651/suppmat.

© 2004 Wiley Periodicals, Inc.

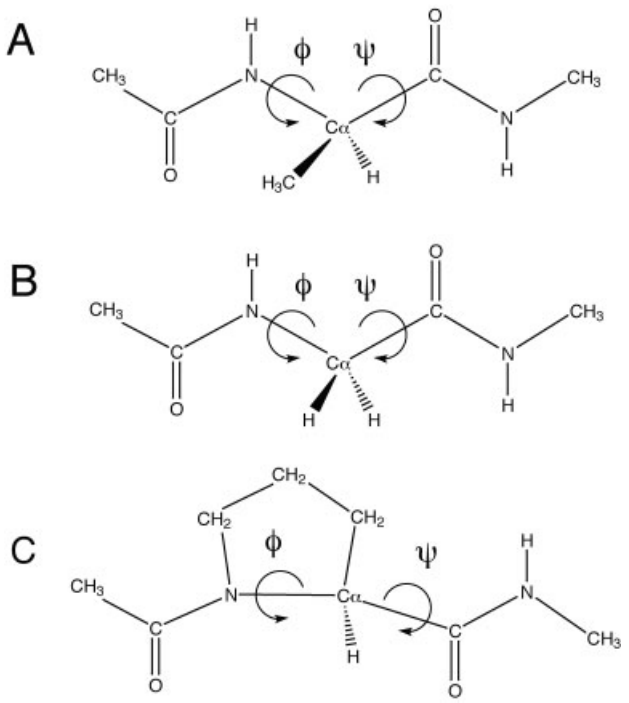

Figure 1. Diagrams of the (A) alanine dipeptide and the (B) glycine dipeptide.

associated with force field bias.[16] For small molecules, limitations are seen for these force fields in the reproduction of quantum mechanical (QM) energetic data on the alanine dipeptide and alanine tetrapeptide.[17] Accordingly, the need for improvements in treatment of the protein backbone via empirical force fields for proteins is evident.

Important benchmarks of the peptide backbone in protein force fields are the alanine and glycine dipeptides (Fig. 1). These molecules contain two peptide bonds surrounding the central ϕ, ψ dihedral angles, the terms that define the Ramachandran diagram.[18,19] As shown by Ramachandran, based on simple steric models the energetics of these model compounds explain, to a large extent, the range of conformations sampled by proteins as observed by crystallographic and NMR experiments. Accordingly, the conformational energies of the dipeptides in the context of empirical force fields have a direct relationship on the behavior of the force fields in modeling studies of proteins. This relationship has motivated a copious number of QM and molecular mechanics (MM)-based studies of the alanine and glycine dipeptides.[17,20–31] Recently, the QM efforts have been extended to include electron correlation[22,32–34] including *ab initio* molecular dynamics on the alanine dipeptide analog,[35] although the full range of ϕ, ψ values have yet to be sampled using these approaches. From these efforts it is clear that improvements in the level of theory of QM studies of the dipeptides do yield different results, supporting the need for additional work in this area.

A significant advance in the optimization of empirical force fields came with the inclusion of macromolecular experimental data as part of the target data. For example, during development of the CHARMM22 all-atom protein force field,[4] data from MD simulations of carboxy-myoglobin (MBCO)[36] were used in the final stages of the optimization of the protein backbone ϕ and ψ dihedral parameters. Other examples include the use of DNA and RNA simulations in the optimization of recent force fields for nucleic acids.[37–39] In applying this approach, however, it is essential to take into account changes in small molecule properties during optimization based on macromolecular target data.[40,41] Such accounting insures that the local properties of the force field remain in proper balance with the global, macromolecular properties.

In this manuscript we present a new version of the CHARMM22 all-atom force field for proteins based on enhanced treatment of the conformational properties of the peptide backbone. This optimization effort includes QM calculations with the treatment of electron correlation effects on the Ramachandran diagrams of the alanine, glycine, and proline dipeptides. The QM data is then used in combination with crystallographic protein target data to improve the treatment of the peptide–backbone force field parameters. This includes the extension of the force field to include energetic terms based on ϕ, ψ dihedral crossterms or grid-based energy correction maps (CMAP), allowing reproduction of the full QM potential energy surfaces for the dipeptides. The latter approach yields quantitative reproduction of any 2D target energy surface, and has recently been shown by us to provide improvements in the treatment of ϕ, ψ conformational properties in protein crystals and in the alanine dipeptide.[42] However, as shown below, exact reproduction of high level QM data for the alanine dipeptide by the force field, when applied to MD simulations of proteins in their crystal environments, leads to systematic deviations in the ϕ, ψ values in α-helical and β-sheet regions. Empirical corrections to the QM targeted energy surface were, therefore, made to overcome these limitations.

Methods

Quantum mechanical calculations were performed with the programs Gaussian98[43] and Jaguar.[44] Geometry optimizations were performed on the alanine, glycine, and proline dipeptides (Fig. 1) at the MP2/6-31G* level of theory with the ϕ (C–N–Cα–C) and ψ (N–Cα–C–N) dihedrals constrained as follows. For the alanine dipeptide the constraints were applied in 15° increments ranging from -180 to 180° for ϕ and ψ, respectively, while for the glycine dipeptide the ϕ range was limited to 0 to 180° due to the symmetry of the molecule associated with the achiral Cα carbon. For the proline dipeptide, ϕ was sampled from -180 through 30°, based on the regions of ϕ sampled in crystal structures (see below). All optimizations were performed to default tolerances in Gaussian98. Local minima were geometry optimized without constraints. Single-point energy calculations were performed at the LMP2 level of theory[45] with the cc-pVDZ, cc-pVTZ and cc-pVQZ(-g) basis sets[46] on the MP2/6-31G* optimized structures. In selected cases, geometry optimizations were performed at the MP2/6-311++G** level of theory with the resulting geometries used for single-point calculations.

Empirical force field calculations were performed using the program CHARMM[47,48] using the CHARMM22 all-atom protein

Table 1. Protein Structures Used in the Force Field Optimization and Testing.

PDB ID	Resolution	Comment	Reference
Proteins used in for crystal simulations			
Crambin[a]	0.94 Å	α-helix, β-sheet	75
1I27	1.02 Å	α-helix, β-sheet, 200 K	76
5PTI	1.8/1.0 Å[2]	α-helix, β-sheet	77
1BZP	1.15 Å	α-helix, 287 K	78
135L	1.3 Å	α-helix, β-sheet, α_L	79
1BYI	0.97 Å	α-helix, parallel β-sheet	80
3EBX	1.4 Å	Antiparallel β-sheet	81
Proteins studied by molecular dynamics in solution			
1GPR	1.9 Å	Glucose permease, X-ray, 162 residues	57
1HIJ	3.0 Å	Interleukin-4, X-ray, 129 residues	56
1UBQ	1.8 Å	Ubiquitin, X-ray, 76 residues	58

[a]Structure obtained from John Kuriyan (personal communication).
[b]The two values represent the resolutions for the neutron and X-ray diffraction experiments, respectively.

force field[4] with the modifications described below. Gas-phase calculations on the dipeptides were performed using infinite cutoffs with geometry optimizations performed to a final gradient $<10^{-6}$ kcal/mol/Å using the adopted-based Newton–Raphson (ABNR) and Newton–Raphson minimization algorithms.[2] Protein simulations were performed using the CHARMM modified TIP3P water model.[49] Electrostatic interactions were calculated with Particle-Mesh Ewald (PME)[50] using a real space cutoff of 10 Å, a grid size of approximately 1 Å and Lennard–Jones (LJ) interactions were determined with force switching[51] over 8 to 10 Å for the crystal calculations. Nonbonded atom lists were maintained to 12 Å and updated heuristically. For the solution simulations, the PME real space cutoff was 8.5 Å, the LJ interactions were switched from 7.5 to 8.5 Å and nonbonded lists were maintained to 10.5 Å. This truncation scheme was used to be consistent with recently reported tests of the CHARMM, AMBER, and OPLS force fields.[52] Integration of Newton's equations of motion was performed using the Leap-Frog algorithm at 300 K, unless noted, in the NPT ensemble[53] with a time step of 2 fs and constraint of all covalent bonds involving hydrogens using SHAKE.[54]

System preparation was performed as follows for the protein crystals presented in Table 1. In all cases the asymmetric unit was employed with water added to fill vacuum space in the crystal and ions (i.e., sodium or chloride) added as required to obtain charge neutrality. When multiple occupancies were present for selected residues, the conformation corresponding to the highest occupation was selected for the calculations. Water molecules were added to the crystals by creating a water box with the approximate dimension of the asymmetric unit and overlaying this onto the crystallograpic coordinates, including all experimentally identified water and ions. All water molecules with their oxygen within 2.8 Å of any crystallographic nonhydrogen atom were then deleted, following which all added water molecules beyond the boundary of the asymmetric unit were deleted. Sodium or chloride ions were then added to yield a neutral system by placing the ions at random positions in the asymmetric unit that were >3 Å from any crystallographic nonhydrogen atom, excluding water, and not within 0.5 Å of any water oxygen or within 3 Å of any previously added ion. The crystallographic nonhydrogen atoms, excluding water, were then subjected to mass weighted harmonic restraints of 5 kcal/mol/Å and the systems were minimized for 200 steepest descent steps in the presence of the crystal environment, using atom truncation for the electrostatic and LJ terms with shifting of the electrostatic terms to 0 at 12 Å, switching the LJ interactions to zero over the range of 10 to 12 Å with the nonbonded list updated heuristically and maintained to 14 Å. These minimized systems were then used to determine the PME screening factor, kappa (approximately 0.33 in all cases) followed by a 200-step ABNR minimization with the harmonic restraints maintained and the electrostatic interactions treated via PME. Final equilibration of the solvent was based on a 20-ps NVT simulation[55] in the presence of the harmonic restraints. An additional 100 steps of ABNR minimization, in the absence of harmonic restraints, was performed on each system prior to the production simulations described above. Production simulations were performed for 1.1 ns, with the initial 100 ps discarded as equilibration with coordinates saved every 5 ps for analysis. For all of the proteins, the N- and C-terminal residues were excluded from the analysis and with BPTI the next to last C-terminal residue (i.e., 57) was also excluded due to anomalously large structural changes in the C-terminus. Simulations were performed at 300 K, unless noted in Table 1.

Details of the individual systems listed in Table 1 follow. Crambin contains four water molecules in addition to the two crystallographic ethanol and water molecules, with the total charge being zero (John Kuryian, personal communcation). 1I27, which is the C-terminal domain of Transcription Factor IIF, was used directly with nine chloride ions added to provide electric neutrality. The experimental crystal structure of 1I27 was obtained at 200 K, and MD simulations were performed at that temperature. BPTI contains a crystallographically defined phosphate and 63 water molecules, with an additional 91 water molecules and four chloride ions. In our previous optimization of the CHARMM all-atom force field, carboxy myoglobin (1MBC),[36] was used as the model protein for empirical optimization of the force field.[48] However, comparison of the average ϕ, ψ values in the helical region for this structure showed the ϕ values to be less negative and the ψ values to be more negative compared to other representative proteins, including a structure of deoxymyoglobin (see Table S1 of the supplemental information). Accordingly, the deoxymyoglobin structure, 1bzp, was substituted for the 1mbc structure in this study. The 1bzp simulation system contained a deoxy heme, three sulfate ions and 154 water molecules identified crystallographically, along with an additional 196 water moleculess and six sodium ions. Turkey Egg Lysozyme contains 114 water molecules in the crystal structure, to which 263 water molecules and nine chloride ions were added. 1byi, dethiobiotin synthase, contains 389 crystallographic water molecules to which 150 water molecules and four sodium ions were added. The final protein, 3ebx, erabu-

Table 2. Relative Energies and ϕ, ψ Dihedral Angles of Selected Conformations of the Alanine Dipeptide.

MP2/6-31g* optimized structures						
				LMP2		
Conformer	ϕ	ψ	MP2/6-31G*	cc-pVDZ	cc-VTZ	cc-VQZ(-g)
$C7_{eq}$	−82.8	77.9	0	0	0	0
C5	−158.4	161.6	1.73	1.45	1.14	1.01
$C7_{ax}$	74.4	−64.1	2.53	2.78	2.58	2.20
β_2	−137.8	22.9	3.28	2.43	2.87	2.84
α_L	63.5	34.8	4.52	4.13	4.46	5.19
α_R[a]	−60	−45	4.91	4.53	4.64	4.50
MP2/6-311++G** optimized structures						
				LMP2		
Conformer	ϕ	ψ	MP2/6-311++G**	cc-pVDZ	cc-VTZ	cc-VQZ(-g)
$C7_{eq}$	−81.9	81.6	0	0	0	0
C5	−158.5	151.5	1.66	1.71	1.38	0.91
$C7_{ax}$	74.3	−57.3	2.33	2.79	2.65	2.06
β_2	−90.7	−7.8	2.83	3.33	2.78	2.51
α_L	63.7	33.6	4.05	4.14	4.48	4.96
α_R[a]	−60	−45	4.00	4.52	4.76	4.27

Energies in kcal/mol and dihedral angles in degrees.
[a] ϕ, ψ dihedral angles constrained to −60, −45.

toxin B, contains a crystallographic sulfate and 112 water molecules; 24 additional water molecules were added to this simulation system.

Solution simulations were performed as previously described,[52] in a truncated octahedron with a minimum solvation layer of 9 Å. The proteins studied included interleukin-4 (1hij, 3.0-Å resolution X-ray structure),[56] domain II of glucose permease (1gpr, 1.9-Å resolution X-ray structure),[57] and ubiquinone (1ubq, 1.8-Å resolution X-ray structure)[58] (Table 1). All simulations were performed for 5 ns, with the analysis performed over the final 3 ns.

Free-energy ϕ, ψ surfaces were produced assuming the dihedral angles were distributed according to a Boltzmann distribution.[59] The experimental surface was based on a collection of high resolution structures from the PDB[60] in which redundant sequences were removed.[61,62] Only those residues with B-factors less than 30 $Å^3$ were included. Calculated free energy surfaces were obtained by collecting the values of all ϕ, ψ dihedral pairs for all residues of the proteins, over the production portions of the MD simulations, constructing distributions from these values and converting the resulting distributions to free energies.[2]

Results and Discussion

Continued optimization of empirical force fields represents an ongoing effort necessitated by the ever-increasing availability of experimental and QM data on the systems for which the force fields were designed. In the case of the CHARMM22 protein all-atom force field several lines of evidence motivated the present work. During the original optimization of the ϕ, ψ dihedral parameters the final adjustments included systematically altering the energy of the α_R conformation of the alanine dipeptide to avoid biasing the α-helical conformation in MD simulations, with MbCO (Table S1) used as the model system. The adjustments lead to CHARMM adequately treating the left side of the alanine dipeptide ϕ, ψ energy surface at the expense of the α_L conformation, whose energy was significantly overestimated (see Table 7 of MacKerell et al.[4]). This limitation was reiterated in a comprehensive QM study of the alanine di- and tetrapeptides.[17] Although limitations with respect to QM data on the alanine dipeptide were indicated, MD simulations on a wide variety of proteins, as reported in the literature, showed no systematic problems in the force field (e.g., see ref. 52). However, two recent problems emerging from MD-based studies motivated our current work. In simulations of lysozyme, order parameters were calculated and compared with NMR data. The calculated values were shown to be significantly lower than those from experiment (M. Buck and M. Karplus, personal communication). These differences were particularly large with glycine residues occupying the α_L conformation. The second problem related to the sampling of the π-helical conformations in a variety of simulations,[10,12,15] as recently discussed.[16]

Taken together, the QM and MD data form a consistent picture. The elevated energy of the α_L conformation in the alanine dipeptide map suggests that the low order parameters in the lysozyme simulation were due to the α_L residues "falling away" from the experimental conformation. Concerning the propensity of the force

field to sample π-helical conformations, this is related to the empirical adjustment of the original CHARMM force field to more accurately treat the α-helical conformation. This procedure led to a decrease in the relative energy of the π- vs. the α-helical conformation, such that the CHARMM22 alanine dipeptide energy surface in the helical region was too "flat" (see below); a similar effect is present in most current force fields.[16] It has recently been shown that this diminished energy difference allows the backbone conformation to sample the π-helical conformations and is an artifact of the force field.[16] These limitations motivated the development and application of a systematic strategy for improving the force field based on reproduction of QM conformational energetics of the three dipeptides and MD simulations of the proteins in Table 1 in their crystal environments.

Quantum Mechanical Calculations

QM studies were undertaken on the alanine, glycine, and proline dipeptides to obtain appropriate target data for the force field parameter optimization. These calculations included determination of the dipeptide potential energy surfaces in 15° increments at the MP2/6-31G* level including full geometry optimization. For the alanine dipeptide, selected conformers were then subjected to energy minimization in the absence of dihedral constraints. The results are shown in Table 2. Geometry optimizations were also performed with the 6-311++G** basis set to test the influence of basis set on the obtained geometries and energies. Analysis of the data presented in Table 2 shows that upon going from the MP2/6-31G* to the LMP2 treatment of electron correlation, with Dunning's correlation corrected basis sets and using the same geometry, significant changes in relative energies can occur. The C5 and α_R conformers are of lower energy when treated with LMP2, the $C7_{ax}$ and α_L energies bracket the MP2 values and the β_2 and α_R LMP2 values are lower than those from the MP2 calculation. In the majority of cases the ordering of the relative energies is not altered upon going to the LMP2 calculations, the only exception being the α_L and α_R conformations, where the α_R is of higher energy at the MP2 and the LMP2/cc-pVDZ and cc-pVTZ levels and of lower energy at the LMP2/cc-pVQZ(-g) level.

Comparison of the relative energies for the MP2/6-311++G** optimized geometries with the MP2/6-31G* values show the MP2 relative energies to be lower with the larger basis set. LMP2 relative energies with the MP2/6-311++G** optimized geometries generally differ by 0.3 kcal/mol or less compared to the MP2/6-31G* geometries, although the β_2 conformer is 0.9 kcal/mol lower with the cc-pVDZ basis set. For the cc-pVTZ and cc-pVQZ(-g) basis sets, the relative energies differ by 0.3 kcal/mol or less, indicating that the MP2/6-31G* optimized geometries are appropriate for determination of the full dipeptide energy surfaces.

The relative energies from our calculations may be compared with data from Vargas et al.[33] In that study, a partial alanine dipeptide surface was obtained at the BLYP/TZVP+ level of theory and full optimization of selected conformations performed at several levels of theory, with the highest being MP2/aug-cc-pVDZ. Using those geometries, energies were calculated at the MP2/aug-cc-pVTZ and MP2/aug-cc-pVQZ levels and the resulting data used to extrapolate to the complete basis set (CBS) limit. At the CBS level the following relative energies were obtained,

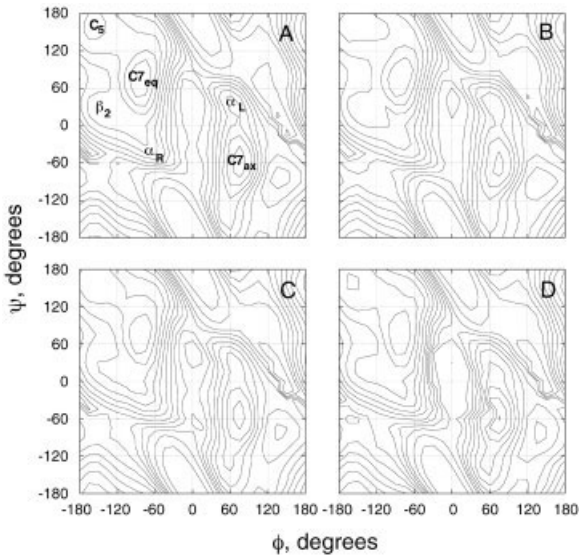

Figure 2. Alanine dipeptide ϕ, ψ energy maps from quantum mechanical calculations at the (A) MP2/6-31G*//MP2/6-31G*, (B) LMP2/cc-pVDZ//MP2/6-31G*, (C) LMP2/cc-pVTZ//MP2/6-31G*, and (D) LMP2/cc-pVQZ(-g)//MP2/6-31G* levels of theory. Energy contours are in 1 kcal/mol increments up to 10 kcal/mol, with two additional contours at 12 and 15 kcal/mol. Energies offset to the $C7_{eq}$ conformer. The approximate locations of the dipeptide conformers discussed in the present work are shown in (A).

C5, 1.39 kcal/mol; $C7_{ax}$ 2.66 kcal/mol; β_2, 3.35 kcal/mol and α_L, 5.19 kcal/mol. Comparison with the LMP2/cc-pVQZ(-g) data in Table 2 shows the agreement to be reasonable, with the present LMP2/cc-pVQZ(-g) energies for the MP2/6-31G* geometries being within 0.5 kcal/mol of the CBS values, while the differences are larger with the MP2/6-311++G** optimized geometries. This comparison further suggests that our determination of the full alanine dipeptide potential energy surface via MP2/6-31G* optimization with single-point energies via LMP2 calculations will yield an adequately converged description of the conformational energetics of this molecule.

The full alanine dipeptide map was, therefore, obtained using MP2/6-31G* geometry optimization. The resulting surface is presented in Figure 2, along with the surfaces based on single-point energy calculations on the MP2/6-31G* optimized geometries using LMP2 to treat electron correlation with the cc-pVDZ, cc-pVTZ, and cc-pVQZ(-g) basis sets. As expected, all of the surfaces are similar, and are consistent with previous QM studies of the alanine dipeptide[22,25,33] However, subtle, but relevant, differences are evident. Upon going from the MP2/6-31G* to the LMP2/cc-pVDZ surface, the energy gradient in the region around the $C7_{eq}$ global minimum decreases and the effect is enhanced upon going to the larger basis sets at the LMP2 level of theory. With respect to the α_R conformation, which corresponds to the α-helical secondary structure in proteins,[63] there is a distinct valley extending from the $C7_{eq}$ region up towards the helical region. As will be shown below, subtle differences in this region of the alanine dipeptide surface when applied to an empirical force field can impact the sampling of the α-helical region in MD simulations.

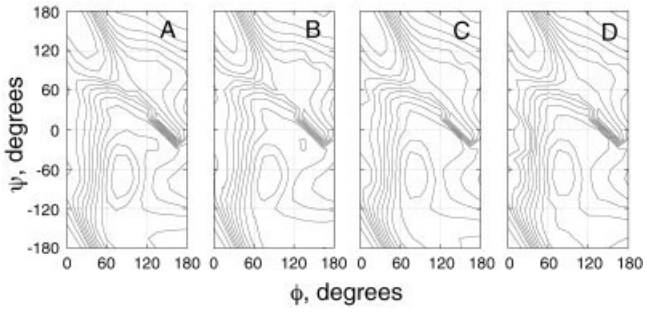

Figure 3. Glycine dipeptide ϕ, ψ energy maps from quantum mechanical calculations at the (A) MP2/6-31G*//MP2/6-31G*, (B) LMP2/cc-pVDZ//MP2/6-31G*, (C) LMP2/cc-pVTZ(-f)//MP2/6-31G*, and (D) LMP2/cc-pVQZ(-g)//MP2/6-31G* levels of theory. Energy contours are in 1 kcal/mol increments up to 10 kcal/mol, with two additional contours at 12 and 15 kcal/mol. Energies offset to the $C7_{ax}$ conformer.

Other regions in the alanine dipeptide that are related to protein secondary structure are the C5 and α_L regions, corresponding to the β-sheet structures and to some reverse or β-turn conformations in proteins, respectively.[63] In all four maps the C5 region is similar, being relatively flat. In the case of the α_L conformation, there is a valley from the $C7_{ax}$ minimum leading up to this region, indicating that the energy barrier between the two minima is rather small. Although the majority of protein residues that assume the α_L conformation are glycines, there is a significant number of nonglycine residues sampling this region, making its proper treatment important.

Potential energy surfaces for the glycine dipeptide at the four QM levels used for the alanine dipeptide are shown in Figure 3. Due to the symmetry of the molecule, only the range of ϕ from 0 to 180° was calculated. A single minimum is present on the surface, corresponding to the $C7_{ax}$ conformation. Comparison of the four surfaces shows them all to be similar, as expected, although some differences are evident. Similar to the $C7_{eq}$ region in the alanine dipeptide, the gradient of the energy is larger with the MP2/6-31G* surface than with calculations based on the LMP2 level of theory. Differences are also present in the portion of the surface leading up to the α_L conformation in the vicinity of $\phi = 60°$, $\psi = 30°$. For the MP2/6-31G* calculations, this conformation is 3.98 kcal/mol above the minimum while with the LMP2 level of theory it is 3.53 kcal/mol, 3.48, and 3.58 kcal/mol for the cc-pVDZ, cc-pVTZ and cc-pVQZ(-g) basis sets, respectively. Thus, as with the alanine dipeptide QM energy surfaces, the glycine dipeptide surfaces are similar for the levels of theory tested, however, some differences are present in regions sampled in protein structures.

QM calculations were also performed on the proline dipeptide (Fig. 1) with the peptide bond in the *trans* conformation. Shown in Figure 4A and 4B are the MP2/6-31G* and LMP2/cc-pVQZ(-g)//MP2/6-31G* surfaces, respectively. No cc-pVDZ or cc-pVTZ surfaces were obtained for the proline dipeptide. Both surfaces have a long narrow minimum energy region in the vicinity of $\phi = -75°$. This corresponds to the restraints placed upon ψ in the proline dipeptide due to the five-membered ring. Notably, upon going to the LMP2 calculation the gradient moving away from the minima decreased. As the regions of ϕ, ψ most occupied in proline residues in protein crystal structures correspond to approximately -60, $-30°$, and -60, 150°, the decreased gradient moving away from the minimum is expected to be important for proper treatment of prolines in proteins.

Empirical Force Field Calculations

To date, optimization of empirical force fields for the protein backbone has typically been based on reproducing the relative energies of selected conformers of the alanine and glycine dipeptides.[4,6,64,65] However, this approach is limited in that it ignores regions of ϕ, ψ conformational space not included in the target dipeptide conformers. These regions include the helical region in proteins as well as higher energy regions not typically observed in proteins. Obviously, correct treatment of the helical region, including the α, 3_{10}, and π helicies, is important for modeling of proteins in native or near-native conformations. Accordingly, it is desirable to treat the entire range of ϕ, ψ values as accurately as possible. Additional optimization of the CHARMM22 empirical force field for the peptide backbone, therefore, used the entire alanine, glycine, or proline dipeptide energy surfaces as target data. Recent work has applied a similar approach to improve treatment of peptide backbone in the Amber force field, although a 30° grid space, vs. the 15° space used here, was employed.[34]

Potential Energy Function

Initial attempts to improve the treatment of the backbone used the current form of the potential energy function (see ref. 39 for the form). Starting with the CHARMM22 force field, it was assumed that only the parameters associated with ϕ and ψ intrastrand dihedrals required optimization (i.e., the C_{-1}–N–Cα–C and N–Cα–C–N_{+1} dihedrals). Considering the force constants and phases for a Fourier series up to and including a sixfold term for each dihedral yields a total of 24 parameters (i.e., a force constant and phase for each term) that are available for optimization. This includes the ability of the phase to assume any value, as currently

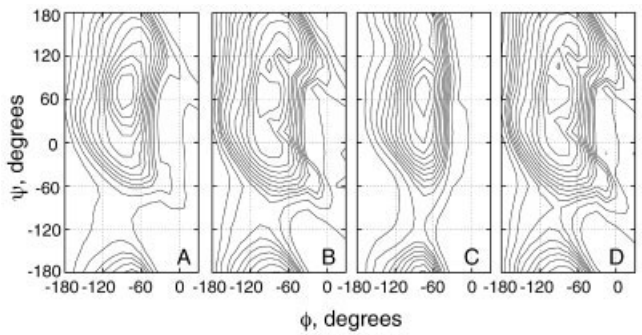

Figure 4. Proline dipeptide ϕ, ψ energy maps from quantum mechanical calculations at the (A) MP2/6-31G*//MP2/6-31G* and (B) MP2/6-31G*// LMP2/cc-pVQZ levels of theory and from empirical calculations using (C) CHARMM22 and the (D) grid-based energy correction map. Energy contours as in Figure 2.

implemented in CHARMM.[66] To perform this optimization a Monte Carlo simulated annealing (MCSA) protocol was applied.[67] In this approach, all 24 parameters were initially set to zero and then randomly sampled and selected based on the Metropolis criteria[68] where the target function was the difference between the empirical and LMP2/cc-pVQZ(-g)//MP2/6-31G* energy surfaces.

The second approach to improving the treatment of the backbone was via the addition of ϕ, ψ crossterms, V_{cross}, to the potential energy function [eq. (1).

$$V_{\text{cross}} = K_{n,m}(1 + \cos(n\phi + m\psi - \delta_{n,m}) \quad (1)$$

In eq. (1) n is the multiplicity of ϕ, m is multiplicity of ψ, $K_{n,m}$ is the force constant for each crossterm, $\delta_{n,m}$ is the phase of each cross term, and n and m are assigned values of 1 through 4, yielding a total of 16 crossterms. These terms were fit in addition to the standard ϕ, ψ dihedrals with all the parameters (i.e., 24 ϕ, ψ dihedral parameters plus 16 $K_{n,m}$ and 16 $\delta_{n,m}$) again optimized via the MCSA protocol. A cross term of a similar form has previously been used as an umbrella potential in potential of mean force calculations on the alanine dipeptide.[69]

The final modification of the CHARMM22 empirical force field we examined was the inclusion of an energy correction map, termed CMAP, to minimize the difference between the empirical and QM target maps. This correction was based on a grid-based interpolation procedure that allows for the energy difference between the target LMP2/cc-pVQZ(-g) and CHARMM22 dipeptide energy surfaces to be reproduced almost exactly. In this protocol, a continuous function is constructed from the grid points through two-dimensional bicubic interpolation according to the following formula:

$$f(\phi, \psi) = \sum_{i=1}^{4} \sum_{j=1}^{4} c_{ij} \left(\frac{\phi - \phi_L}{\Delta_\phi} \right)^{i-1} \left(\frac{\psi - \psi_L}{\Delta_\psi} \right)^{j-1} \quad (2)$$

The cubic nature of the interpolating polynomial guarantees that a set of coefficients and first derivatives can be found so that the first derivatives are smooth and the second derivatives are continuous across grid boundaries, as required for MM applications. For each grid rectangle the coefficients are determined according to ref. 70 from the grid values at each of the four corner grid points, as well as the first derivatives,

$$\frac{\partial f}{\partial \phi}, \frac{\partial f}{\partial \psi}$$

and cross-derivatives

$$\frac{\partial f^2}{\partial \phi \partial \psi}$$

at the grid points. As a first approximation, derivatives at the grid points may be obtained as finite differences from neighboring grid points. However, in general, this only guarantees continuous but not smooth first derivatives, which is not sufficient for molecular mechanics applications. This could be remedied with a higher order of interpolation, but the necessary algebra quickly becomes rather complicated and it is not trivial to determine the appropriate coefficients. As a more convenient alternative one can use bicubic *spline* interpolation to generate a set of grid derivatives that will lead to smooth first derivatives if used in the simple bicubic interpolation algorithm described above.[70] The more expensive bicubic spline interpolation of the entire grid only needs to be done once, and the resulting values can be precomputed and stored for a given grid.

In this interpolation scheme only the grid cell where an interpolating point is located and its immediate neighbors are involved. The coefficients c_{ij} need to be calculated only once for all grid cells of a given grid, and can be stored and reused for computational efficiency. Then only eq. (2) needs to be computed for each function evaluation, which is typically faster than a conventional cosine series expansion. The partial first and second derivatives of eq. (2) with respect to ϕ and ψ provide the analytical derivatives at a given interpolation point. Using the chain rule they can then be applied with respect to cartesian coordinates[66,71] analogous to single torsion functions to obtain atomic forces and second derivatives. This algorithm has been implemented in the program CHARMM, version 31.

Table 3. RMS Differences in the Relative Energies between the Empirical and Quantum Mechanical LMP2/cc-pVQZ(-g)// MP2/6-31G* Potential Energy Surfaces for the Alanine, Glycine and Proline Dipeptides.[a]

Empirical model	Alanine	Glycine	Proline
CHARMM22	2.47	1.85	2.67
MCSA fit	1.29	1.29	
MCSA fit, PDB weight	1.38	1.39	
MCSA fit, crossterms	0.69	0.91	
MCSA fit, crossterms, PDB weight	0.78	1.05	
Grid correction	0.04	0.04	0.15
Grid + empirical correction	0.48	0.56	

[a]Energies in kcal/mol. Zero energies were adjusted to minimize the RMS differences, which were calculated over the entire ϕ, ψ map for the alanine dipeptide (15° increments, yielding 625 points), over ϕ = 0 to 180°, inclusive, for the glycine dipeptide (325 points) and over ϕ = −180 to 30°, inclusive for the proline dipeptide (375 points). MCSA fit indicates the Monte Carlo Simulated Annealing procedure to fit the ϕ, ψ dihedral parameters (see text) in the absence or presence of the crossterms or PDB weighting.

Dipeptide Empirical Gas-Phase Calculations

Application of the three approaches to improve the CHARMM22 energy function initially targeted the LMP2/cc-pVQZ(-g)//MP2/6-31G* QM maps for the alanine and glycine dipeptides. Later efforts included the proline dipeptide (see below). Presented in Table 3 are the root-mean-square (RMS) differences of CHARMM22 and the three new models with respect to the QM data for the entire surfaces (i.e., 625 and 325 points for the alanine and glycine dipeptides, respectively). As is evident, significant improvements in the reproduction of the QM data by the force field

was made via the MCSA procedure in the context of the present form of the potential energy function. Although, in principle, the CHARMM22 force field could have previously been optimized to the current level, it would have been difficult without targeting the newly available energy surfaces. Previous optimization efforts targeted the relative energies of five or six conformations of the alanine dipeptide (e.g., those in Table 2), such that application of MCSA with 24 parameters being optimized is clearly an underdetermined problem; such a scenario would lead to artifacts in other parts of the map not constrained in the fitting procedure. Extension of the potential energy function to include crossterms, leads to a significant gain in the ability to reproduce the QM data. This is evidenced by the decrease in the RMS differences from 1.29 to 0.69 kcal/mol and from 1.29 to 0.91 kcal/mol for the alanine and glycine dipeptides, respectively (Table 3). Thus, targeting the full dipeptide surfaces both without and with extension of the potential energy function allows for use of the MCSA procedure, yielding significant improvements in the quality of the fit to the gas phase data.

MCSA fitting to the potential function both without and with the crossterms was also performed targeting the QM dipeptide surfaces by weighting the QM data with ϕ, ψ probability distributions from the PDB.[61,62] This was performed to enhance the quality of the fit in the region of the dipeptide maps corresponding to those sampled in the native structures of proteins. A weighting factor, $W = \log\{(50{,}000 \cdot P_{\phi,\psi}) + 1.1\}$, where $P_{\phi,\psi}$ is the probability for a particular ϕ, ψ coordinate, was applied to each ϕ, ψ point in the target energy surface. As may be seen in Table 3, inclusion of PDB weighting leads to good agreement with the QM data, although the bias towards the sampled regions leads to the agreement being slightly less good than the unweighted fits.

As will be discussed below, additional improvement in the quality of the fit of the force field to the QM data beyond that obtained with the fourfold crossterms was deemed necessary. Improvements in the agreement could simply be obtained via extension to five or more ϕ, ψ crossterms in the context of eq. (1). However, this leads to 50 or more parameters associated with the crossterms plus the additional 24 terms associated with the standard ϕ, ψ dihedrals. This large number of parameters is starting to approach the number of data points in the target surfaces, which may lead to problems in the MCSA fitting. Instead, a ϕ, ψ energy correction term for the difference between the CHARMM22 and QM surfaces based on a grid-interpolation protocol was implemented [eq. (2)]. Inclusion of the interpolation-based energy correction term yields near perfect agreement with the QM maps as evidenced by the RMS differences of 0.04 kcal/mol in Table 3. Clearly, agreement between the empirical model and the QM data can be improved via enhanced sampling of the parameters via the MCSA approach and with extension of the potential energy function via inclusion of ϕ, ψ crossterms. However, use of the grid correction leads to almost exact reproduction of the QM map. In addition, a grid correction approach allows for more direct control of the energy surface when applying empirical adjustments to improve agreement with condensed-phase experimental data (see below).

The empirical maps from CHARMM22 and the three, non-PDB weighted, empirical models (Table 3) are presented in Figure 5 for the alanine dipeptide, respectively. In the CHARMM22

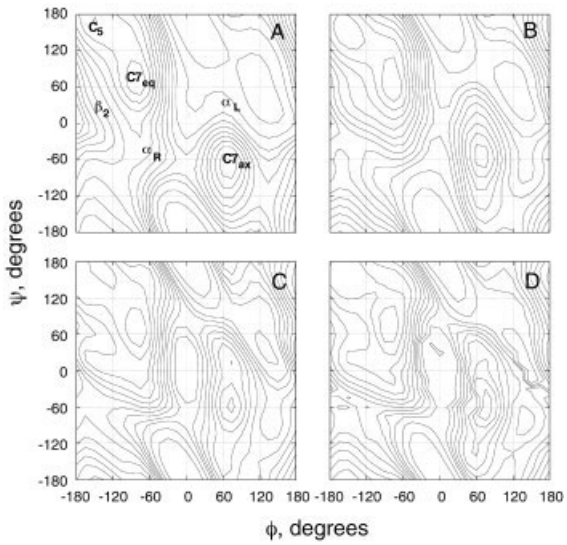

Figure 5. Alanine dipeptide ϕ, ψ energy maps from empirical calculations with (A) CHARMM22, (B) MCSA optimized ϕ, ψ parameters, (C) MCSA optimized ϕ, ψ parameters with crossterms, and (D) the spline-based energy correction. Energy contours as in Figure 2.

surfaces, the overall shape is in agreement with the QM surfaces (Fig. 2); however, significant differences are present. For example, in the alanine dipeptide surface (Fig. 5a) the broad plateau in the QM maps (Fig. 2) in the vicinity of $-90°$, 0° is not present, and the shape of the surface in the helical region differs. This includes the CHARMM22 surface being relatively flat in the α-helical region as ψ decreases (i.e., from $-60°$, -45 to $-60°$, $-75°$), in contrast to the QM surfaces, where a significant increase in energy occurs. The lack of a significant energy rise in this region has been shown to lead to artificial sampling of π-helices in MD simulations, and is a common feature in a number of other empirical force field.[16] In addition, the $C7_{ax}$ region is more spherical and the energy gradient larger in the CHARMM22 map compared to the QM surfaces, leading to the overestimation of the α_L conformer of both the alanine and glycine dipeptides. Additional optimization of ϕ, ψ dihedral parameters via MCSA yields an overall improvement in the shape of the empirical surface (Fig. 5b) compared to the target QM surface (Fig. 2d). However, the energy differences between the α- and π-helical conformations (i.e., -60, $-75°$, and -60, $-45°$, respectively) is still underestimated in the alanine dipeptide, being only 2.9 kcal/mol vs. the QM value of 5.3 kcal/mol, while the α_L relative energy is still overestimated at 6.6 kcal/mol vs. the QM value of 5.2 kcal/mol. Extension of the force field to include the crossterms combined with the MCSA fit yielded the expected improvements (Fig. 5c). The plateau region around the β_2 conformer (~ -90, 0°) is now well defined, the valley leading to the helical region is improved and the shape of the $C7_{ax}$ region is more extended, all in better agreement with the QM surface. However, the α–π helical energy difference is still underestimated at 4.3 kcal/mol and, interestingly, the α_L energy is now underestimated at 4.3 kcal/mol. This level of disagreement motivated the alternative extension of the force field to include the interpolation-based energy correction term [eq. (2)]. The resulting ϕ, ψ map (Fig. 5d)

Table 4. Average ϕ, ψ Differences between the MD Average and Crystal Values Averaged Over All Residues.

Protein	CHARMM22 ϕ, ψ	Grid correction ϕ, ψ	Grid + empirical correction ϕ, ψ
Lysozyme	3.4 ± 2.1, −3.2 ± 2.3	1.4 ± 1.0, −1.6 ± 1.0	−1.0 ± 0.9, 0.5 ± 1.0
Crambin	3.1 ± 1.6, −2.6 ± 2.1	2.0 ± 1.4, −1.2 ± 1.3	1.2 ± 1.0, −1.0 ± 1.4
BPTI	0.4 ± 1.8, −2.0 ± 1.7	3.0 ± 1.2, −2.9 ± 1.0	−0.3 ± 1.0, 0.1 ± 0.8
1I27	2.0 ± 1.3, −2.6 ± 1.2	0.5 ± 1.0, −1.3 ± 0.9	0.0 ± 0.9, −1.0 ± 0.7
1BZP	0.1 ± 1.2, 0.0 ± 1.4	−3.1 ± 0.7, 3.3 ± 0.7	−2.1 ± 0.9, 2.0 ± 0.9
3EBX	4.9 ± 2.0, −3.6 ± 2.0	5.7 ± 2.6, −5.8 ± 2.3	2.4 ± 2.0, −2.6 ± 1.8
1BYI	1.5 ± 1.6, 0.3 ± 1.8	0.1 ± 1.6, −1.0 ± 1.5	−1.9 ± 1.3, −0.5 ± 1.2

Angles in degrees and errors are the standard deviations. MD averages from the final 1-ns of 1.1-ns simulations in the crystal environment.

is nearly identical to the QM target map (Fig. 2b), consistent with the RMS difference of 0.04 kcal/mol in Table 3. This includes excellent agreement with the α–π helical and α_L relative energies discussed above. Clearly, the proposed grid-interpolation energy correction approach allows for reproduction of any (e.g., QM) target surface, and allows for testing of the impact of exact reproduction of a gas-phase QM dipeptide surface on protein structure and dynamics obtained in MM calculations. This approach is reminiscent of a QM-based umbrella potential approach to correct dipeptide free energy surfaces;[25] however, it has the distinct advantage of being applicable to all aspect of MM-based calculations on peptides and proteins.

The importance of the extension of the potential energy function to the glycine and proline dipeptides is also evident. With the glycine dipeptides a similar scenerio to that with the alanine dipeptide was observed. As shown in Figure S1 of the supplemental material, compared to the QM surface in Figure 3d, additional optimization of the ϕ, ψ dihedrals via the MCSA followed by the extension of the cross-terms [eq. (1)] lead to improved agreement with the QM target data. However, the grid correction approach [eq. (2)] was required to accurately reproduce all the subtle features of the QM surface with the empirical model. With the proline map, the application of the grid correction method yields an empirical surface (Fig. 4d) that is in much better agreement with the target QM data (Fig. 4b) compared to the CHARMM22 surface (Fig. 4c). Application of the MCSA parameter optimization using the CHARMM energy function, with and without the ϕ, ψ cross-terms [eq. (1)] was not performed on the proline dipeptide.

Empirical Optimization of ϕ, ψ Surfaces Targeting Crystal Simulations

Although it is desirable for a force field to reproduce gas-phase conformational energies of model compounds, for an empirical force field designed for studies of macromolecules in the condensed phase it must also reproduce experimental macromolecular target data. Accordingly, simulations of the proteins listed in Table 1 were performed including explicit treatment of the crystal environment. Inclusion of the crystal environment is expected to allow for a one to one comparison with X-ray–based target data.[72] The primary target data from these simulations were the experimentally determined ϕ, ψ values for the individual proteins as well as reproduction of a ϕ, ψ free energy surface based on a survey of the PDB.[61,62] In addition, RMS fluctuations about ϕ and ψ were analyzed along with RMS differences of the Cartesian coordinates with respect to the crystal structures.

Presented in Table 4 are the average ϕ, ψ differences between the MD and crystal structures for the three empirical models and average ϕ ψ differences for the helical and sheet regions are shown in Tables 5 and 6, respectively. For CHARMM22, the average ϕ, ψ differences are typically 3° or less, with the exception of 3EBX, and there is a trend where average ϕ differences are positive while the ψ values are negative. Use of the grid correction method to treat ϕ, ψ energetics yields average differences that are smaller than those of CHARMM22 in the majority of cases. Although averaging over all residues indicates a slight improvement associated with the grid correction, analysis of the average differences in the helical and sheet regions indicated some undesirable trends. Average helical differences in Table 5 show the grid corrected ϕ values to be systematically negative. Analysis of the average ϕ, ψ differences in the sheet regions (Table 6) shows the opposite trend, where the ϕ values are systematically positive in the simulations using the grid correction. A similar trend occurs with CHARMM22. These systematic trends in the grid corrected surfaces indicate that although high-level QM conformational energies can be reproduced almost exactly, there are still systematic deviations with respect to experimental crystallographic structures when the model is applied to proteins.

Supporting the trends of these average values in the CHARMM22 and grid-corrected simulation results are comparison of PMFs from a survey of ϕ, ψ values in the PDB and from the crystal simulations. Presented in Figure 6 are the respective PMFs. In CHARMM22 (Fig. 6B) the shapes of the minimum energies regions (i.e., sheet, α-helical and α_L) are significantly more spherical than those observed in the survey. This difference speaks to the inherent limitations in the potential energy function with only Fourier series for the dihedral terms used to treat the ϕ, ψ energy surface. Upon using the grid corrected surfaces for the MD simulations the overall shape of the surface (Fig. 6C) is in better agreement with the PDB PMF. For example, the three minimum regions are more elongated. However, systematic differences are

Table 5. Average ϕ, ψ Differences between the MD Average and Crystal Values Averaged Over All Residues in the Helical Region.

Protein	CHARMM22 ϕ, ψ	Grid correction ϕ, ψ	Grid + empirical correction ϕ, ψ
Lysozyme (75)	1.0 ± 1.9, -10.3 ± 1.9	-2.7 ± 1.0, -2.7 ± 1.3	-1.1 ± 1.0, -2.1 ± 1.1
Crambin (27)	1.3 ± 1.5, -5.6 ± 2.9	-3.7 ± 0.9, -0.3 ± 1.7	-0.9 ± 1.1, 1.1 ± 1.6
BPTI (21)	-0.1 ± 2.0, -8.3 ± 3.5	-2.9 ± 1.2, -3.0 ± 1.5	-1.0 ± 1.4, -1.7 ± 1.2
1I27 (38)	0.9 ± 1.0, -3.6 ± 1.3	-2.9 ± 0.8, 1.5 ± 0.7	-0.4 ± 0.9, -0.7 ± 0.6
1BZP (133)	-1.1 ± 1.1, -1.1 ± 1.5	-4.0 ± 0.6, 2.3 ± 0.7	-1.9 ± 0.7, 1.0 ± 0.8
3EBX (6)	2.1 ± 6.1, -12.2 ± 9.0	-4.5 ± 7.6, 1.2 ± 12.0	-1.2 ± 4.4, -3.7 ± 5.6
1BYI (110)	-1.2 ± 1.3, -3.4 ± 2.4	-6.3 ± 1.4, 0.8 ± 1.2	-3.5 ± 1.1, 0.3 ± 1.2

Angles in degrees and errors are the standard deviations. MD averages from the final 1-ns of 1.1-ns simulations in the crystal environment. Helical region defined as ϕ between $-30°$ and $-150°$ and ψ between $-90°$ and $30°$ in the crystal structure. Value in parentheses following the protein name is n, the number of residues in the helical region in each protein.

still evident. In the α-helical region there is oversampling of negative ϕ values while in the sheet region there is a tendency towards more positive ϕ values. These trends are consistent with the results in Tables 5 and 6, respectively, emphasizing the inherent limitations in the use of the QM ϕ, ψ surfaces directly for MD simulations.

To better understand the contributions of individual residue types to the systematic trends discussed above, PMFs were produced for all residues excluding glycine and proline (Fig. 7), all glycines (Fig. 8) and all prolines (Fig. 9). For all nonglycine and proline residues the systematic trends observed in Figure 6 are still evident for the CHARMM22 and the grid-corrected surfaces. To correct for these trends, empirical optimization of the alanine-based surface was undertaken. This optimization procedure focused on (1) improving the "shape" of the PMFs in the sheet, α-helical, and α_L regions; and (2) obtaining the proper relative energies of the C5 vs. α_R alanine dipeptide conformations to ensure the sampling of the α-helical and sheet regions was correct. The adjustments were performed in an iterative fashion where selected points in the energy correction map were manually adjusted, the seven crystal MD simulations performed and the overall PMFs (e.g., Fig. 7) as well as the average ϕ, ψ differences for the individual proteins (Tables 4, 5, and 6) were compared to experiment. The process was continued until satisfactory agreement with the crystal results was obtained. It should be noted that the use of a grid-correction approach, vs. the direct use of ϕ, ψ crossterms [eq. (1)] allows for direct optimization of the ϕ, ψ surfaces. Use of ϕ, ψ crossterms requires a fitting approach, such that manual adjustment to fine tune the surface is difficult.

A similar empirical adjustment procedure was applied to glycine residues via optimization of the glycine dipeptide correction surface. This was motivated by deviations of the grid corrected surface (Fig. 8C) from the PDB PMF (Fig. 8A). For example, the grid corrected surface showed additional sampling in the vicinity of $90°$, $-60°$ compared to the PDB data. However, with proline, the quality of the grid-corrected PMF (Fig. 9C) was deemed to be in adequate agreement with the PDB-based PMF (Fig. 9A) and additional adjustments were not needed. It should also be noted that the relatively small number of proline residues in the seven

Table 6. Average ϕ, ψ Differences between the MD Average and Crystal Values Averaged Over All Residues in the Sheet Region.

Protein	CHARMM22 ϕ, ψ	Grid correction ϕ, ψ	Grid + empirical correction ϕ, ψ
Lysozyme (36)	-4.0 ± 3.2, 9.4 ± 5.2	7.7 ± 2.0, 1.2 ± 1.8	-1.8 ± 2.3, 2.2 ± 2.2
Crambin (13)	4.3 ± 3.7, -0.1 ± 2.8	10.9 ± 2.5, -4.4 ± 2.5	5.4 ± 1.7, -3.5 ± 1.8
BPTI (29)	1.1 ± 2.1, 2.9 ± 1.4	6.4 ± 1.2, -2.3 ± 1.1	0.4 ± 1.2, 1.3 ± 1.2
1I27 (26)	3.0 ± 3.1, -2.8 ± 2.6	5.3 ± 2.1, -5.5 ± 2.0	0.8 ± 2.1, -2.8 ± 1.6
1BZP (11)	11.7 ± 6.3, 10.5 ± 4.7	0.7 ± 6.0, 9.8 ± 4.9	-7.9 ± 7.7, 11.6 ± 7.9
3EBX (44)	4.7 ± 2.4, -3.0 ± 2.0	7.5 ± 3.2, -8.0 ± 2.2	3.7 ± 2.6, -3.9 ± 2.0
1BYI (90)	2.2 ± 2.2, 3.2 ± 2.3	7.7 ± 2.9, -6.5 ± 2.8	0.7 ± 2.1, -2.3 ± 1.6

Angles in degrees and errors are the standard deviations. MD averages from the final 1-ns and 1.1-ns simulations in the crystal environment. Sheet region defined as ϕ between $-30°$ and $-180°$ and ψ between $60°$ and $180°$ in the crystal structure. Value in parentheses following the protein name is n, the number of residues in the sheet region in each protein.

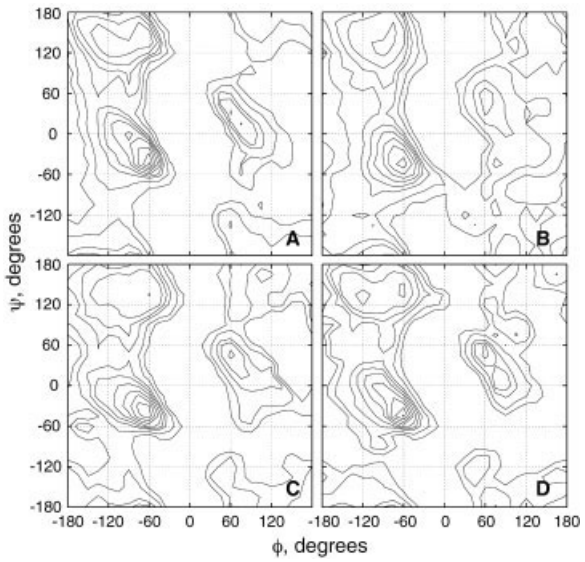

Figure 6. ϕ, ψ free energy surfaces (PMFs) for all residues based on probability distributions from the (A) PDB and MD simulations of the seven proteins in the top part of Table 1 using the (B) CHARMM22, (C) grid correction, and (D) grid + empirical correction force fields. Energy contours are −6, −5.5, −5, −4.5, −4, −3.5, −3, −2, −1 kcal/mol.

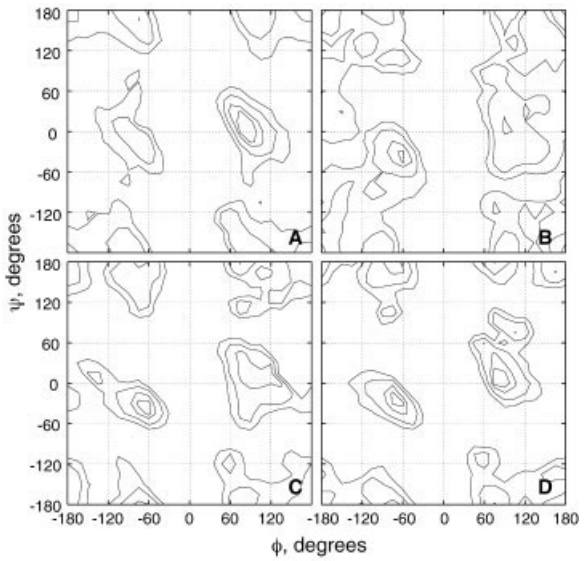

Figure 8. ϕ, ψ free-energy surfaces (PMFs) for all glycine residues based on probability distributions from the (A) PDB and MD simulations of the seven proteins in the top part of Table 1 using the (B) CHARMM22, (C) grid correction, and (D) grid + empirical correction force fields. Energy contours are −3.5, −3, −2, −1 kcal/mol.

test set of protein crystal structures would make empirical optimization difficult for this residue.

Presented in panel D of Figures 6–9 are the PMFs using the final optimized surfaces (i.e., the empirically optimized alanine and glycine surfaces and the QM based proline surface) for all residues, all nonglycine and nonproline residues, glycine residues, and proline residues, respectively. In all cases, these surfaces are in good qualitative agreement with the respective PDB-based PMFs (A panels). Moreover, analysis of the average ϕ, ψ values for the seven individual crystals in Tables 4, 5, and 6 indicate that the empirical surface is in quantitative agreement with the experimental data. This is indicated by the average differences typically being in the range of the standard deviations, with the largest exceptions occurring when the number of a particular residue type is low (e.g., there are only 11 and 13 residues in the sheet region of 1bzp and crambin, respectively). In addition, there are no significant trends in the average differences, indicating the overall

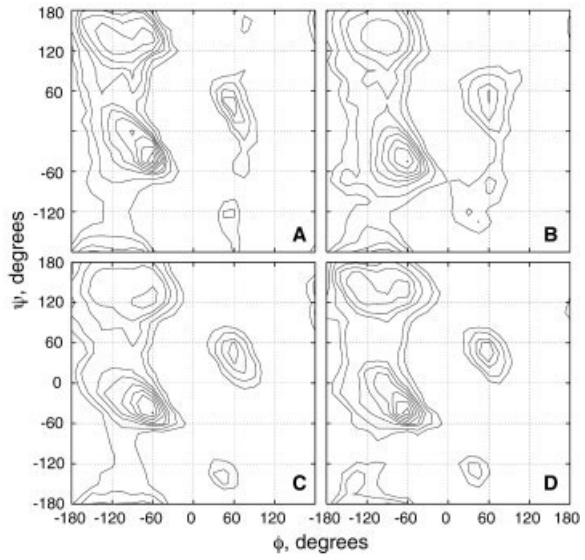

Figure 7. ϕ, ψ free-energy surfaces (PMFs) for all residues excluding glycine and proline based on probability distributions from the (A) PDB and MD simulations of the seven proteins in the top part of Table 1 using the (B) CHARMM22, (C) grid correction, and (D) grid + empirical correction force fields. Energy contours are −6, −5.5, −5, −4.5, −4, −3.5, −3, −2, −1 kcal/mol.

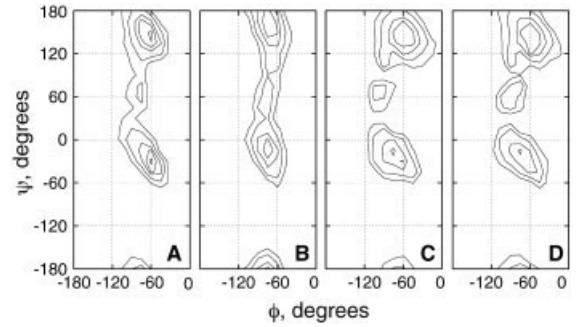

Figure 9. ϕ, ψ free-energy surfaces (PMFs) for all proline residues based on probability distributions from the (A) PDB and MD simulations of the seven proteins in the top part of Table 1 using the (B) CHARMM22, (C) grid correction, and (D) grid + empirical correction force fields. Energy contours are −3.5, −3, −2, −1 kcal/mol.

Table 7. ϕ, ψ RMS Fluctuations Averaged Over All Residues from the Crystal MD Simulations.

Protein	CHARMM22 ϕ, ψ	Grid correction ϕ, ψ	Grid + empirical correction ϕ, ψ
Lysozyme	20.5 ± 1.6, 22.2 ± 1.8	14.8 ± 0.6, 13.7 ± 0.6	13.6 ± 0.6, 13.6 ± 0.6
Crambin	14.3 ± 1.1, 15.1 ± 1.4	14.1 ± 1.0, 12.5 ± 0.9	11.5 ± 0.8, 11.8 ± 1.1
BPTI	16.2 ± 1.5, 16.0 ± 1.3	14.2 ± 0.6, 12.2 ± 0.6	12.7 ± 0.5, 11.0 ± 0.5
1I27	12.1 ± 0.7, 11.5 ± 0.7	10.9 ± 0.7, 9.5 ± 0.7	9.7 ± 0.6, 8.1 ± 0.5
1BZP	14.5 ± 0.9, 15.1 ± 1.1	11.9 ± 0.5, 11.2 ± 0.5	11.6 ± 0.7, 11.6 ± 0.7
3EBX	18.7 ± 1.2, 17.7 ± 1.3	21.8 ± 1.7, 18.8 ± 1.7	17.5 ± 1.3, 15.0 ± 1.2
1BYI	17.3 ± 1.4, 17.9 ± 1.4	17.3 ± 1.5, 16.0 ± 1.3	14.1 ± 1.3, 12.6 ± 0.9

RMS fluctuations in degrees and the errors represent the standard deviations.

balance of the force field. The only exception to this occurs with helical ϕ values (Table 6), though the magnitude of most of the values are within the standard deviation. Thus, the grid-correction method combined with empirical adjustments allowed for development of a force field for the protein backbone that accurately treats the overall surface, taking into account condensed phase contributions not included in the QM ϕ, ψ energy surfaces.

Beyond analysis of the ϕ, ψ averages and distributions, RMS fluctuations of ϕ and ψ for the individual proteins along with RMS differences of the Cartesian coordinates with respect to the experimental crystal structures were obtained. Presented in Table 7 are the ϕ, ψ RMS fluctuations. In all cases, with the exception of 3ebx, going from CHARMM22 to the grid corrected surface, lead to a decrease in the RMS fluctuations. Upon empirical optimization of the grid correction surface additional decreases in the RMS fluctuations occurred in the majority of cases, including a decrease in those from the 3ebx crystal simulations. The decreased RMS fluctuations, which were not part of the target data for the optimization, suggest that more accurate treatment of the overall ϕ, ψ energy surface via the grid corrected method leads to greater stability in the sampling of ϕ, ψ. Notable are the significant decreases with lysozyme, where problems with calculated order parameters being to small with respect to experiment have been observed (M. Buck and M, Karplus, personal communication). The decreased RMS fluctuations suggest that this problem may, in part, be ameliorated by the new model. However, rigorous evaluation of this behavior requires more detailed comparison with experimental data, such as NMR order parameters.

Concerning RMS differences, comparison of the CHARMM22 and grid + empirical correction values for the seven crystals (Table 8), indicate only minor improvement in the optimized model. This suggests that the improvements in ϕ, ψ improve the treatment of the overall 3D structure of the proteins. Additional support for this is observed in the structural changes found in our MD simulations of test proteins in solution (see below). However, the relatively small differences in the Cartesian RMS differences indicate this term alone to not be an appropriate metric for force field optimization.

The impact of the empirical adjustments to the grid corrected surface on the alanine dipeptide ϕ, ψ map is shown in Figure 10, which included the LMP2/cc-pVQZ(-g)//MP2/6-31G* and grid + empirical correction force field surfaces. It is evident that the overall integrity of the QM map is maintained in the empirically optimized surface. Supporting this are RMS differences of the energy of the entire surfaces for the alanine and glycine dipeptides, showing overall deviations of approximately 0.5 kcal/mol (Table 3). These deviations are less than those obtained using any of the other models (e.g., MCSA fit, crossterms) to treat ϕ, ψ. Comparison of energies and ϕ, ψ values for the selected alanine dipeptide conformers are presented in Table 9. With the final model the largest difference occurred in the C5 conformer, whose relative energy was −1.00 kcal/mol, vs. the QM value of 1.01 kcal/mol. Of

Table 8. Average RMS Differences of the Backbone (Bkb) and Side Chain (Sdc) Nonhydrogen Atoms.

Protein	CHARMM22 Bkb, Sdc	Grid correction Bkb, Sdc	Grid + empirical correction Bkb, Sdc
Lysozyme	1.18, 1.74	0.97, 1.63	0.95, 1.55
Crambin	0.58, 1.17	0.57, 0.96	0.56, 0.97
BPTI	0.94, 1.63	0.77, 1.17	0.93, 1.20
1I27	0.62, 1.05	0.66, 1.00	0.60, 0.95
1BZP	1.06, 1.71	0.80, 1.45	0.94, 1.52
3EBX	0.65, 1.09	0.69, 1.11	0.65, 0.99
1BYI	1.52, 1.81	1.26, 1.64	1.25, 1.62

RMS differences in Å. RMS fluctuations about the average values were 0.01 Å or less in all cases.

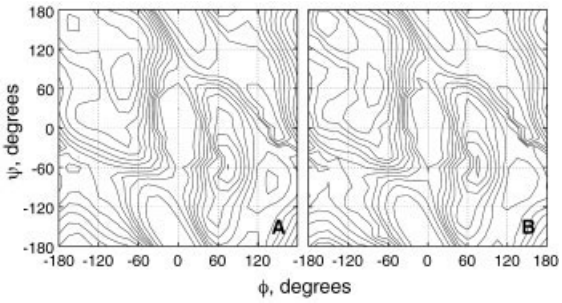

Figure 10. Alanine dipeptide ϕ, ψ energy maps from the (A) MP2/6-31G*// LMP2/cc-pVQZ(-g) QM level of theory and the (B) grid + empirical correction force field model. Energy contours are in 1-kcal/mol increments up to 10 kcal/mol with two additional contours at 12 and 15 kcal/mol.

Table 9. Relative Energies and ϕ, ψ Values of Selected Conformers of the Alanine Dipeptide.

Conformer	ϕ	ψ	LMP2/cc-VQZ(-g)// MP2/6-31G*	C22	Grid	Grid + empirical correction
$C7_{eq}$	−82.8	77.9	0	0	0	0
C5	−158.4	161.6	1.01	0.92	0.97	−1.00
$C7_{ax}$	74.4	−64.1	2.20	2.05	1.96	1.52
β_2[a]	−137.8	22.9	2.84	5.96	2.82	2.37
α_L[a]	63.5	34.8	5.19	10.97	5.15	4.71
α_R[a]	−60	−45	4.50	4.78	4.48	3.23
			ϕ/ψ values			
$C7_{eq}$			−82.8/77.9	−81.3/70.6	−81.7/75.2	−77.3/66.3
C5			−158.4/161.6	−151.5/170	−159.8/164	−159.0/165.1
$C7_{ax}$			74.4/−64.1	69.7/−67.7	78.2/−55.8	78.2/−55.8

Energies in kcal/mol and dihedral angles in degrees.
[a] ϕ, ψ dihedral angles constrained to the quantum mechanical values.

the remaining conformations, the largest difference with respect to the QM data is for the α_R conformer. This difference reflects adjustments of the $C7_{eq}$ conformer relative to the C5 conformer, such that the difference between the C5 and α_R conformations is 4.23 kcal/mol vs. the QM value 3.49 kcal/mol. As stated above, this greater energy difference in the grid + empirical correction model reflects the need to enhance sampling of the C5 region in the crystal simulations. Previous QM studies on the alanine dipeptide using several reaction field models reported the relative energy of the C5 conformation in the presence of solvent to range from −0.1 to −1.0 kcal/mol.[26] This lowering of energy is consistent with a model where increased interactions of the C5 conformer with the environment lead to stabilization of that conformation. Ideally, such effects would be represented directly by the force field upon moving from a gas to a condensed phase environment. However, the responsiveness to environmental changes is limited by the form of the potential energy function, such that the differences had to be directly incorporated into the model, leading to the decreased C5 energy. The relevance of such a phenomena to force field development has been discussed previously.[40,73,74] Thus, to reproduce crystallographically observed ϕ, ψ distributions it is necessary to deviate from the gas phase alanine dipeptide potential energy surface. Notable is the generally better agreement of the CHARMM22 energies with the QM data compared to the grid + empirical correction results. This is associated with the use of only these conformations in the optimization of the CHARMM22 force field, such that reproduction of the selected QM data was enhanced at the expense of reproduction of the entire ϕ, ψ surfaces.

Solution MD Simulations

Final tests of the force field parameters were based on solution MD simulations of the three proteins listed in the latter portion of Table 1. The first two proteins were selected based on their use in a recent comparison of the AMBER, OPLS, and CHARMM22 force fields,[52] and the final protein, ubiquitin, was selected to include an additional high resolution protein in the test set whose structure was obtained via X-ray crystallography. All simulations were run for 5 ns, with the final 3 ns used for analysis; in the previous study the simulations were run for 2 ns. Comparison of the average ϕ, ψ differences shows the grid + empirical correction model to give significant improvements in all cases (Table 10). In addition, ϕ, ψ PMFs from the solution simulation, shown in Figure 11, indicate that the overall distribution is in significantly better agreement with the PDB based surface (Fig. 6A) compared to CHARMM22. With respect to RMS fluctuations (Table 11) the grid + empirical

Table 10. Average ϕ, ψ Differences between the MD Average and Experimental Values Averaged Over All Residues, Helical Region Residues, and Sheet Region Residues for the Solution MD Simulations.

	All residues	
	CHARMM22	Grid + empirical correction
Protein	ϕ, ψ	ϕ, ψ
1gpr	5.3 ± 2.1, −2.6 ± 2.3	−0.2 ± 0.9, 0.0 ± 0.8
1hij	6.2 ± 1.5, −4.2 ± 2.4	3.2 ± 1.5, −2.0 ± 2.0
1ubq	5.2 ± 1.9, −5.0 ± 2.6	1.2 ± 1.2, −2.0 ± 1.9
	Helical residues	
1gpr	5.8 ± 2.9, −10.3 ± 4.8	2.5 ± 1.6, −1.6 ± 1.8
1hij	5.1 ± 1.2, −7.6 ± 2.0	3.1 ± 1.2, −2.5 ± 1.7
1ubq	0.9 ± 2.7, −7.2 ± 3.9	0.1 ± 1.6, −1.7 ± 1.8
	Sheet residues	
1gpr	3.9 ± 2.0, 1.4 ± 2.5	−0.9 ± 1.3, 0.7 ± 1.0
1hij	6.0 ± 5.9, 8.1 ± 6.0	0.0 ± 5.6, 5.9 ± 6.0
1ubq	3.9 ± 1.8, −2.9 ± 2.0	1.5 ± 1.7, 0.4 ± 1.7

Dihedral angle differences in degrees and the errors represent the standard deviations.

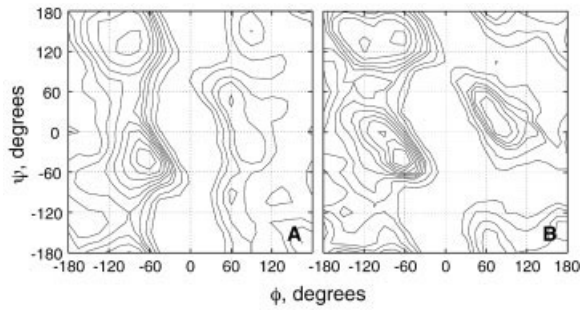

Figure 11. ϕ, ψ free-energy surfaces (PMFs) for all residues based on probability distributions from the three solution MD simulations using the (A) CHARMM22 and (B) grid + empirical correction force fields. Energy contours are −6, −5.5, −5, −4.5, −4, −3.5, −3, −2, −1 kcal/mol.

correction results yielded smaller values than CHARMM22, further indicating increased stability in the new model. Finally, RMS differences of the Cartesian coordinates (Table 12) show significant improvements with the new model for 1gpr and 1hij, with 1ubq having similar results for the new model and CHARMM22. Thus, the developed force field shows improvements in the treatment of the backbone conformational properties and in the overall structural properties as compared to CHARMM22. These results support the quality of the grid + empirical correction model for MD simulations of proteins.

Conclusion

Motivated by limitations in the CHARMM22 all-atom protein force field in reproducing both QM and experimental protein structural properties, additional optimization of the force field was undertaken. Initial efforts to augment the force field within the context of the current form of the potential energy lead to only incremental improvements. This lead to extension of the potential energy function to initially include ϕ, ψ dihedral crossterms before finally selecting a grid-based energy correction procedure allowing for reproduction of any 2D target energy surfaces.[42] Such an approach has the advantage of allowing for rigorous testing of, for example, a quantum mechanics-based energy surface in the context of condensed phase MM calculation.

Table 11. ϕ, ψ RMS Fluctuations Averaged Over All Residues from the Solution MD Simulations.

Protein	CHARMM22 ϕ, ψ	Grid + empirical correction ϕ, ψ
1gpr	23.7 ± 1.9, 25.6 ± 2.0	15.5 ± 0.7, 13.7 ± 0.6
1hij	18.3 ± 1.2, 22.8 ± 2.1	16.8 ± 1.2, 18.9 ± 1.9
1ubq	20.3 ± 2.4, 21.6 ± 2.6	15.2 ± 0.8, 14.3 ± 1.6

Dihedral angle RMS fluctuations in degrees and the errors represent the standard deviations.

Table 12. Average RMS Differences of the Backbone (Bkb) and Side Chain (Sdc) Nonhydrogen Atom Cartesian Coordinates for the Solution MD Simulations.

	CHARMM22		Grid + empirical correction	
Protein	Bkb	Sdc	Bkb	Sdc
1gpr	1.26	2.20	0.90	1.75
1hij	1.69	3.16	1.33	2.64
1ubq	1.15	2.03	1.20	2.01

RMS differences in Å.

In the present work it is shown that direct use of a high-level QM-based energy surface for the peptide backbone yields generally improved agreement with experimental ϕ, ψ distributions compared to the CHARMM22 force field (Table 4), although systematic deviations in ϕ and ψ in the helical (Table 5) and sheet (Table 6) regions are evident (Fig. 6). Therefore, empirical corrections to the grid correction were undertaken, correcting, to a large extent, the systematic deviations. Empirical corrections were deemed necessary for both the alanine and glycine dipeptides while the QM-based correction surface was used directly for proline; although the use of the QM-based surface for proline was based, in part, on the presence of only seven prolines in the crystal structures used in the present study. The final grid + empirical correction model also yielded decreased average RMS fluctuations of ϕ and ψ (Table 7) and Cartesian-based RMS differences (Table 8) were generally improved. Similar improvements were observed in MD simulations of three proteins in solution (Tables 10 to 12).

In the context of the CHARMM potential energy function, the need to empirically correct the QM dipeptide ϕ, ψ surfaces emphasizes the importance of fitting the region of ϕ, ψ space sampled in the native structures of proteins to produce parameters appropriate for MM studies of such systems. In CHARMM22 it was necessary to sacrifice the quality of the α_L relative energy to get the energetics of the remaining portion of the alanine dipeptide map in satisfactory agreement with QM data as well as yield good agreement with the experimental ϕ, ψ distributions in MbCO. However, in that work details of the treatment of the sheet region were not investigated and, as discussed above, there appear to be limitations in the MbCO helical structure. When the potential energy function is extended, as done in the present study, it is possible to reproduce the entire QM alanine dipeptide map with the MM model in the gas phase. However, when this is performed, accurate treatment of condensed phase ϕ, ψ distributions in both the helical and sheet regions is not achieved, requiring the empirical adjustments described above. It is therefore evident that current potential energy functions in use cannot simultaneously treat both the gas and condensed phases with high accuracy. Accordingly, quantifying the quality of a force field designed for condensed phase simulations solely using gas-phase QM data is inappropriate. As potential energy functions are further extended to include electronic polarizability, as well as other terms, it will be interesting to see if the current gap between accurate treatment of gas-phase and condensed-phase properties can be overcome.

Acknowledgments

Computational support from the Department of Defense High Performance Computing and the National Partnership of Advanced Computational Infrastructure are acknowledged. Also, computing support from the DOD is gratefully acknowledged.

References

1. Becker, O. M.; MacKerell, J., A.D.; Roux, B.; Watanabe, M., Eds.; Computational Biochemistry and Biophysics; Marcel-Dekker, Inc.: New York, 2001.
2. Brooks, C. L., III; Karplus, M.; Pettitt, B. M. Proteins: A Theoretical Perspective of Dynamics, Structure, and Thermodynamics; John Wiley & Sons: New York, 1988.
3. Neria, E.; Fischer, S.; Karplus, M. J Chem Phys 1996, 105, 1902.
4. MacKerell, A. D., Jr.; Bashford, D.; Bellott, M.; Dunbrack, R. L., Jr.; Evanseck, J.; Field, M. J.; Fischer, S.; Gao, J.; Guo, H.; Ha, S.; Joseph, D.; Kuchnir, L.; Kuczera, K.; Lau, F. T. K.; Mattos, C.; Michnick, S.; Ngo, T.; Nguyen, D. T.; Prodhom, B.; Reiher, I., W. E.; Roux, B.; Schlenkrich, M.; Smith, J.; Stote, R.; Straub, J.; Watanabe, M.; Wiorkiewicz–Kuczera, J.; Yin, D.; Karplus, M. J Phys Chem B 1998, 102, 3586.
5. Jorgensen, W. L.; Tirado–Rives, J. J Am Chem Soc 1988, 110, 1657.
6. Cornell, W. D.; Cieplak, P.; Bayly, C. I.; Gould, I. R.; Merz, K. M.; Ferguson, D. M.; Spellmeyer, D. C.; Fox, T.; Caldwell, J. W.; Kollman, P. A. J Am Chem Soc 1995, 117, 5179.
7. van Gunsteren, W. F.; Billeter, S. R.; Eising, A. A.; Hünenberger, P. H.; Krüger, P.; Mark, A. E.; Scott, W. R. P.; Tironi, I. G. Biomolecular Simulation: The GROMOS96 Manual and User Guide; BIOMOS b.v.: Zürich, 1996.
8. Némethy, G.; Gibson, K. D.; Palmer, K. A.; Yoon, C. N.; Paterlini, G.; Zagari, A.; Rumsey, S.; Scheraga, H. A. J Phys Chem 1992, 96, 6472.
9. Ponder, J. Washington University School of Medicine: St. Louis, MO, 2002.
10. Shirley, W. A.; Brooks, C. L., III. Proteins 1997, 28, 59.
11. Sajot, N.; Garnier, N.; Genest, M. Theor Chem Acc 1999, 101, 67.
12. Mahadevan, J.; Lee, K. H.; Kuczera, K. J Phys Chem B 2001, 105, 1863.
13. Lee, K. H.; Benson, D. R.; Kuczera, K. Biochemistry 2000, 39, 13737.
14. Hiltpold, A.; Ferrara, P.; Gsponer, J.; Caflisch, A. J Phys Chem B 2000, 104, 10080.
15. Pak, Y.; Jang, S.; Shin, S. J Chem Phys 2002, 116, 6831.
16. Feig, M.; MacKerell, A. D., Jr.; Brooks, C. L., III. J Phys Chem B 2002, 107, 2831.
17. Beachy, M. D.; Chasman, D.; Murphy, R. B.; Halgren, T. A.; Friesner, R. A. J Am Chem Soc 1997, 119, 5908.
18. Ramachandran, G. N.; Ramakrishnan, C.; Sasisekharan, V. J Mol Biol 1963, 7, 95.
19. Ramachandran, G. N.; V., S. Adv Protein Chem 1968, 23, 283.
20. Weiner, S. J.; Kollman, P. A.; Case, D. A.; Singh, U. C.; Ghio, C.; Alagona, G.; Profeta, S.; Weiner, P. J Am Chem Soc 1984, 106, 765.
21. Head–Gordon, T.; Head–Gordon, M.; Frisch, M. J.; Brooks, C., III; Pople, J. Int J Quantum Chem Quantum Biol Symp 1989, 16, 311.
22. Head–Gordon, T.; Head–Gordon, M.; Frisch, M. J.; Brooks, C. L., III; Pople, J. A. J Am Chem Soc 1991, 113, 5989.
23. Böhm, H.-J. J Am Chem Soc 1993, 115, 6152.
24. Gould, I. R.; Cornell, W. D.; Hiller, I. H. J Am Chem Soc 1994, 116, 9250.
25. Ono, S.; Kuroda, M.; Higo, J.; Nakajima, N.; Nakamura, H. J Comput Chem 2002, 23, 470.
26. Cortis, C. M.; Langlois, J.-M.; Beach, M. D.; Friesner, R. A. J Chem Phys 1996, 105, 5472.
27. Grant, J. A.; Williams, R. L.; Scheraga, H. A. Biopolymers 1990, 30, 929.
28. Schäfer, L.; Newton, S. Q.; Momany, F.; Klimkowski, V. J. J Mol Struct (Theochem) 1991, 232, 275.
29. Perczel, A.; Angyan, J. G.; Kajtar, M.; Viviani, W.; Rivail, J. L.; Marcoccia, J. F.; Csizmadia, I. G. J Am Chem Soc 1991, 113, 6256.
30. Brooks, C. L., III; Case, D. A. Chem Rev 1993, 93, 2487.
31. Dudek, M. J.; Ponder, J. J Comput Chem 1994, 16, 791.
32. Frey, R. F.; Coffin, J.; Newton, S. Q.; Ramek, M.; Cheng, V. K. W.; Momany, F. A.; Schäfer, L. J Am Chem Soc 1992, 114, 5369.
33. Vargas, R.; Garza, J.; Hay, B. P.; Dixon, D. A. J Phys Chem A 2002, 106, 3213.
34. Duan, Y.; Wu, C.; Chowdhury, S.; Lee, M. C.; Xiong, G.; Zhang, W.; Yang, R.; Ceiplak, P.; Luo, R.; Lee, T.; Caldwell, J.; Wang, J.; Kollman, P. J Comput Chem 2003, 24, 1999.
35. Wei, D.; Guo, H.; Salahub, D. R. Phys Rev E 2001, 64, 011907.
36. Kuriyan, J.; Wilz, S.; Karplus, M.; Petsko, G. J Mol Biol 1986, 192, 227.
37. Langley, D. R. J Biomol Struct Dyn 1998, 16, 487.
38. Cheatham, T. E., III; Cieplak, P.; Kollman, P. A. J Biomol Struct Dyn 1999, 16, 845.
39. Foloppe, N.; MacKerell, A. D., Jr. J Comput Chem 2000, 21, 86.
40. MacKerell, A. D., Jr.; Banavali, N. B.; Foloppe, N. Biopolymers 2001, 56, 257.
41. MacKerell, A. D., Jr. In Computational Biochemistry and Biophysics; Watanabe, M., Ed.; Marcel Dekker, Inc.: New York, 2001, p. 7.
42. MacKerell, A. D., Jr.; Feig, M.; Brooks, C. L., III. J Am Chem Soc 2004, 126, 698.
43. Frisch, M. J.; Trucks, G. W.; Schlegel, H. B.; Scuseria, G. E.; Robb, M. A.; Cheeseman, J. R.; Zakrzewski, V. G.; Montgomery, J. A., Jr.; Stratmann, R. E.; Burant, J. C.; Dapprich, S.; Millam, J. M.; Daniels, A. D.; Kudin, K. N.; Strain, M. C.; Farkas, O.; Tomasi, J.; Barone, V.; Cossi, M.; Cammi, R.; Mennucci, B.; Pomelli, C.; Adamo, C.; Clifford, S.; Ochterski, J.; Petersson, G. A.; Ayala, P. Y.; Cui, Q.; Morokuma, K.; Malick, D. K.; Rabuck, A. D.; Raghavachari, K.; Foresman, J. B.; Cioslowski, J.; Ortiz, J. V.; Baboul, A. G.; Stefanov, B. B.; Liu, G.; Liashenko, A.; Piskorz, P.; Komaromi, I.; Gomperts, R.; Martin, R. L.; Fox, D. J.; Keith, T.; Al-Laham, M. A.; Peng, C. Y.; Nanayakkara, A.; Gonzalez, C.; Challacombe, M.; Gill, P. M. W.; Johnson, B.; Chen, W.; Wong, M. W.; Andres, J. L.; Gonzalez, C.; Head–Gordon, M.; Replogle, E. S.; Pople, J. A.; Gaussian, Inc.: Pittsburgh, PA, 1998.
44. Jaguar. Schrödinger, Inc.: Portland, OR, 1991–2000.
45. Saebø, S.; Tong, W.; Pulay, P. J Chem Phys 1993, 98, 2170.
46. Woon, D. E.; Dunning, T. H., Jr. J Chem Phys 1993, 98, 1358.
47. Brooks, B. R.; Bruccoleri, R. E.; Olafson, B. D.; Swaminathan, S.; Karplus, M. J Comput Chem 1983, 4, 187.
48. MacKerell, A. D., Jr.; Brooks, B.; Brooks, C. L., III; Nilsson, L.; Roux, B.; Won, Y.; Karplus, M. In Encyclopedia of Computational Chemistry; Schreiner, P. R., Ed.; John Wiley & Sons: Chichester, 1998, p. 271.
49. Jorgensen, W. L. J Phys Chem 1983, 87, 5304.
50. Darden, T. A.; York, D.; Pedersen, L. G. J Chem Phys 1993, 98, 10089.
51. Steinbach, P. J.; Brooks, B. R. J Comput Chem 1994, 15, 667.
52. Price, D. J.; Brooks, C. L., III. J Comput Chem 2002, 23, 1045.
53. Feller, S. E.; Zhang, Y.; Pastor, R. W.; Brooks, R. W. J Chem Phys 1995, 103, 4613.
54. Ryckaert, J.-P.; Ciccotti, G.; Berendsen, H. J. C. J Comp Phys 1977, 23, 327.
55. Nosé, S. J Chem Phys 1984, 81, 511.

56. Mueller, T.; Oehlenschlaeger, F.; Buehner, M. J Mol Biol 1995, 247, 360.
57. Liao, D.-I.; Kapadia, G.; Reddy, P.; M.H. Saier, J.; Reizer, J.; Herzberg, O. Biochemistry 1991, 30, 9583.
58. Vijay–Kumar, S.; Bugg, C. E.; Cook, W. J. J Mol Biol 1987, 194, 531.
59. McQuarrie, D. A. Statistical Mechanics; Harper & Row: New York, 1976.
60. Berman, H. M.; Battistuz, T.; Bhat, T. N.; Bluhm, W. F.; Bourne, P. E.; Burkhardt, K.; Feng, Z.; Gilliland, G. L.; Iype, L.; Jain, S.; Fagan, P.; Marvin, J.; Padilla, D.; Ravichandran, V.; Schneider, B.; Thanki, N.; Weissig, H.; Westbrook, J. D.; Zardecki, C. Acta Crystallogr D 2002, 58(Pt 6 Pt 1), 899.
61. Dunbrack, R. L., Jr.; Cohen, F. E. Protein Sci 1997, 6, 1661.
62. Dunbrack, R. L., Jr.: Philadelphia, 2002. http://www.fccc.edu/research/labs/dunbrack/pisces/.
63. Creighton, T. E. Proteins: Structures and Molecular Properties; W.H. Freeman and Co.: New York, 1993.
64. Momany, F. A.; McGuire, R. F.; Burgess, A. W.; Scherage, H. A. J Phys Chem 1975, 79, 2361.
65. Jorgensen, W. L.; Gao, J. J Am Chem Soc 1988, 110, 4212.
66. Blondel, A.; Karplus, M. J Comput Chem 1996, 17, 1132.
67. Kirkpatrick, S.; Gelatt, C. D. J.; Vecchi, M. P. Science 1983, 220, 671.
68. Metropolis, N. A.; Rosenbluth, A. W.; Rosenbluth, M. N.; Teller, A. H.; Teller, E. J Chem Phys 1953, 21, 1087.
69. Smith, P. E. J Chem Phys 1999, 111, 5568.
70. Press, W. H.; Flannery, B. P.; Teukolsky, S. A.; Vetterling, W. T. Numerical Recipes: The Art of Scientific Computing; Cambridge University Press: Cambridge, 1988.
71. Niketic, S. R.; Rasmussen, K. The Consistent Force Field: A Documentation; Springer-Verlag: Berlin, 1977.
72. Walser, R.; Hünenberger, P. H.; van Gunsteren, W. F. Proteins 2002, 48, 327.
73. Kollman, P. A.; Dill, K. A. J Biomol Struct Dyn 1991, 8, 1103.
74. Gibson, K. D.; Scheraga, H. A. J Biomol Struct Dyn 1991, 8, 1109.
75. Hendrickson, W. A.; Teeter, M. M. Nature 1981, 290, 107.
76. Kamada, K.; De Angelis, J.; Roeder, R. G.; Burley, S. K. Proc Natl Acad Sci USA 2001, 98, 3115.
77. Wlodawer, A.; Walter, J.; Huber, R.; Sjölin, L. J Mol Biol 1984, 180, 301.
78. Kachalova, G. S.; Popov, A. N.; Bartunik, H. D. Science 1999, 284.
79. Harata, K. Acta Crystallogr D 1993, D49, 497.
80. Sandalova, T.; Schneider, G.; Kack, H.; Lindqvist, Y. Acta Crystallogr D 1999, 55, 610.
81. Smith, J. L.; Corfield, P. W. R.; Hendrickson, W. A.; Low, B. W. Acta Crystallogr A 1988, 44, 357.